European Polymer Journal 159 (2021) 110732

Contents lists available at ScienceDirect

European Polymer Journal

journal homepage: www.elsevier.com/locate/europolj

Bisphosphonate-functionalized poly(amido amine) crosslinked 2-hydroxyethyl methacrylate hydrogel as tissue engineering scaffold

Melek Naz Guven [a], Burcu Balaban [a], Gozde Demirci [b], Havva Yagci Acar [b], Oguz Okay [c], Duygu Avci [a,*]

[a] Department of Chemistry, Bogazici University, 34342 Bebek, Istanbul, Turkey
[b] Department of Chemistry, Koc University, 34450 Sariyer, Istanbul, Turkey
[c] Department of Chemistry, Istanbul Technical University, Maslak, 34469 Istanbul, Turkey

ARTICLE INFO

Keywords:
Hydrogels
Bisphosphonates
Poly(amido amine)s
Biomineralization
Crosslinker

ABSTRACT

The first water soluble, bisphosphonate (BP, not bisphosphonic acid)-functionalized poly(amido amine) macromer (PAA-BP) is synthesized and used as a crosslinker for synthesis of a biodegradable and biocompatible hydrogel for tissue engineering scaffolds. The synthesis of PAA-BP is performed in three steps, the first two giving the control macromers (PAA-NHBoc and PAA-NH_2): i) Michael addition reaction of *N,N'*-methylene bisacrylamide and *N*-Boc-1,6-hexanediamine (acrylamide/amine ratios of 1.2), ii) deprotection of Boc-protected amine groups, iii) Michael addition reaction of the amine groups with tetraethyl vinylidene bisphosphonate. The degree of BP substitution is 50% and molecular weight of the PAA-BP macromer is found to be 4800 g/mol. These macromers are incorporated into hydrogels by copolymerization with 2-hydroxyethyl methacrylate and the influence of bisphosphonate functionality on hydrogel properties; degradation, swelling, mechanical and mineralization, is investigated. The mineralization abilities, hence the mechanical properties of the hydrogels are strongly influenced by the BP functionality; PAA-BP forming strong (E = 83 ± 1 kPa) hydrogel-apatite composites, PAA-NH_2 also working to a lesser degree (E = 54 ± 3 kPa). Cytocompatibility of the hydrogels is observed on Saos-2 human osteosarcoma, U-2 OS human bone osteosarcoma epithelial, C2C12 mouse myoblast muscle and NIH mouse embryonic fibroblast 3T3 cells. PAA-BP crosslinked hydrogels facilitate adhesion of C2C12 cells after mineralization. In summary, BP-functionalized hydrogel may have a potential impact on bone tissue engineering.

1. Introduction

Bone tissue engineering (BTE) requires 3D porous scaffolds which mimic bone structure, providing a system for cells to attach, proliferate, and form an extracellular matrix (ECM) [1]. Biocompatibility, biodegradability, mechanical strength, adjustable pore size, facility of cell adhesion and proliferation are essential properties for suitable scaffolds. Polymer-based bone scaffolds possess most of these properties, which can be controlled by composition and preparation of the materials, e.g. modifying their functional groups [2–5]. Among these polymer-based bone scaffolds, hydrogels are especially promising candidates.

Hydrogels are highly hydrated three-dimensional polymer networks and present unique properties making them favorable for many clinical applications [6]. They can exhibit behavior responsive to external stimuli such as pH and temperature [7,8]. The structures of hydrogels are very similar to that of the ECM, making them good candidates for tissue engineering scaffolds. A variety of synthetic and natural polymers may be used to form them [9–13].

There are different strategies for achieving bone mineralization via hydrogels in BTE applications. One of these strategies is adding bioactive inorganic phases, including bioglasses or calcium phosphates to form inorganic-hydrogel composites which mimic the function of natural bone and provide nucleation point for hydroxyapatite (HAP) formation [14]. Another frequent method is to functionalize the backbone of hydrogels with anionic groups such as phosphoric acid (PO_4) [15,16,17], phosphonic acid (PO_3H_2), bisphosphonic acid ($(OH)_2$-(O)P-C-P(O)-$(OH)_2$) [18,19,20] or carboxylic acid (COOH) [21]. These negatively charged groups act as nucleation points to Ca cations and enhance HAP crystal deposition [22,23]. Among these anionic groups, bisphosphonic acids (BPAc) stand out. In the literature, the term

* Corresponding author.
E-mail address: avcid@boun.edu.tr (D. Avci).

https://doi.org/10.1016/j.eurpolymj.2021.110732
Received 27 June 2021; Received in revised form 13 August 2021; Accepted 24 August 2021
Available online 26 August 2021

bisphosphonate is usually used as shorthand for bisphosphonic acid and is abbreviated as BP. Since in this work we have to distinguish between the bisphosphonate and bisphosphonic acid functional groups we will abbreviate them as BP and BPAc, respectively. Bisphosphonic acids are structural analogues of naturally existing pyrophosphate with increased chemical and enzymatic stability and they are commonly used in the treatment of bone diseases [24]. Also BPAc's have strong and reversible binding affinity to calcium ions as well as to the bone mineral HAP [18,25–28]. Furthermore, the choice of functional groups also effects cellular behavior, such as adhesion, spreading, proliferation and differentiation [29–35]. For example, amine groups (—NH_2) on the surfaces were observed to support cell adhesion and growth better than some other functionalities in a certain context [31].

The objective of this work is to evaluate for the first time the effect of bisphosphonate (BP) functional group (again, not bisphosphonic acid, which unfortunately is also abbreviated as BP in relevant works in the literature) with the aim of developing biomimetic systems for bone tissue engineering. Therefore a BP-functionalized poly(amido amine) (PAA)-based crosslinker was used in the synthesis of a 2-hydroxyethyl methacrylate (HEMA)-based hydrogel. The performance of the scaffold was compared to a control hydrogel (PAA-NH_2-crosslinked). Although hydrogels with (bis)phosphonic acid functional groups were investigated as tissue engineering scaffolds [18,25–28,36], there are just a few reports about phosphonate functionalized ones in the literature [37,38], no bisphosphonate one to the best of our knowledge.

PAAs are a class of synthetic polymers with *tert*-amine functional groups generally obtained by aza-Michael-type addition of primary or secondary amines to bisacrylamides. PAAs satisfy the basic requirements for tissue engineering scaffolds because they are biodegradable depending on their specific structure, and nontoxic despite their polycationic nature [20,39–41]. Further functionalization of PAAs with side chain substituents can be easily achieved using different bisacrylamides and amines. Some of these substituents can mimic molecules like oligopeptides and proteins, e.g. RGD, which play an important role in providing the receptorial sites for cell adhesion. For example, Ferruti et al. studied RGD-mimicking PAA-based hydrogels with tunable degradation rates and improved mechanical and biological properties by copolymerization with HEMA [42,43]. The choice of a poly-HEMA-based hydrogel is motivated by the fact that its water content is similar to living tissues and it has hemocompatibility, shows resistance to degradation [44] and has micro porous structure (polymerization-induced phase separation) which is an advantageous morphology for tissue engineering scaffolds [45].

After synthesis of the BP-functionalized PAA-crosslinked HEMA hydrogel, we investigated its swelling, degradation, mechanical, toxicity and cell interaction properties. We demonstrated its mineralization ability and compared it with the gels prepared by using the intermediate versions of macromers as crosslinkers where the functionalization is —NH_2 and -NHBoc respectively, instead of BP.

2. Experimental section

2.1. Materials

N,N′-methylene bisacrylamide (MBA), *N*-Boc-1,6-hexanediamine, trifluoroacetic acid (TFA), 2-hydroxyethyl methacrylate (HEMA), 2-hydroxy-4′-(2-hydroxyethoxy)-2-methylpropiophenone (Irgacure 2959), all other chemicals and solvents were purchased at the highest quality from Sigma-Aldrich and used as received. Tetraethyl vinylidene bisphosphonate was prepared by the method of Degenhardt and Burdsall [46]. Dulbecco's Modified Eagle Medium (DMEM) (with l-glutamine and high glucose (4.5 g/l)) with and without phenol red, McCoy 5A modified cell medium, penicillin/streptomycin (pen-strep), fetal bovine serum (FBS) and trypsin-EDTA were purchased from Diagnovum, Ebsdorfergrund (Germany). Thiazolyl blue tetrazolium bromide (MTT) was provided by Gold Biotechnology (USA) and phosphate buffered saline (PBS) tablets were provided by BBI Life Sciences (China). 48 and 96-Well cell culture plates were obtained from Nest Biotechnology (China). 4% Paraformaldehyde solution was obtained from Santa Cruz Biotechnology, Inc (USA). 4′,6-diamidino-2-phenylindole (DAPI) and fluorescein isothiocyanate (FITC)-labelled phalloidin were purchased from Sigma (USA). Saos-2 human osteosarcoma cells and NIH 3T3 mouse embryonic fibroblast cells were a kind gift of Prof. Dr. Halil Kavakli (Department of Molecular Biology and Genetics, Koc University, Istanbul, Turkey). U-2 OS human bone osteosarcoma epithelial cells were a kind gift of Prof. Dr. Devrim Gozuacık (Department of Molecular Biology, Genetics and Bioengineering, Sabanci University, Istanbul, Turkey). C2C12 (mouse myoblast muscle) cells were purchased from ATCC (USA).

2.2. Methods

^{1}H and ^{13}C NMR spectra were taken in deuterated methanol (MeOD) or deuterated water (D_2O) on a Varian Gemini 400 MHz spectrometer at ambient temperature and chemical shifts δ are given in ppm with respect to the residual water peak, $\delta = 4.80$ ppm. A Fourier transform infrared spectrometer (FTIR) (Thermo Scientific Nicolet 380) equipped with a diamond ATR was used to characterize the macromers and analyze the mineralization of hydrogels. Differential scanning calorimetry (DSC) (TA Instruments Q100) was used to determine the glass transition temperatures (T_g) of the macromers. The morphologies of the hydrogel samples were examined with scanning electron microscopy (SEM) (FEI-Philips XL30) with an accelerating voltage of 10.0 kV after sputter coating of the lyophilized samples with a platinum layer. The energy-dispersive X-ray spectroscopy (EDX) analysis was used to identify the elemental composition of materials. Degradation studies were done using an incubator shaker (VWR) operating at 37 °C and 200 rpm. The mineral content of the cryogels was determined from thermogravimetric measurements (TGA). TGA studies were performed using a Perkin Elmer STA 6000 machine. Samples were heated up to 700 °C at a rate of 10 °C/min under nitrogen atmosphere. Also, crystallographic properties of the apatite formed were analyzed by using X-ray powder diffraction (XRD) analysis (Rigaku-D/MAX-Ultima diffractometer).

2.3. Synthesis of PAA Macromers (PAA-NHBoc, PAA-NH_2 and PAA-BP)

Synthesis of PAA-BP macromer was carried out in three steps. In the first step, MBA (293 mg, 1.90 mmol) and *N*-Boc-1,6-hexanediamine (342.5 mg, 1.58 mmol) were dissolved in water/methanol mixture (v/v = 3/1, 3.48 mL in total) (1 M) and the mixture was stirred about 4 days at 50 °C under N_2. After the removal of the solvents under vacuum, the residue was washed three times with diethyl ether (5 mL). A white precipitate was filtered off and dried under vacuum to give pure product (PAA-NHBoc) in 90% yield. In the second step, to a solution of the product from the first step (613 mg, 0.13 mmol) in dichloromethane (DCM) (1.5 mL), TFA (0.1 mL, 1.3 mmol) was added slowly at 0 °C under N_2 and the reaction mixture was stirred overnight at room temperature. After the removal of the volatiles under vacuum, the residue was dissolved in water and the pH of the aqueous solution was adjusted to 8.0 with 2.5 M NaOH solution. Then the solution was lyophilized, the remaining solid was dissolved in a small amount of methanol and added dropwise into diethyl ether (50 mL) under stirring. The precipitate was filtered off to give the pure product (PAA- NH_2) as a white solid in 80% yield. In the third step, PAA-NH_2 (250 mg, 1 equiv.) and tetraethyl vinylidene bisphosphonate (300 mg, 15 equiv.) were stirred in DCM (2 mL) at room temperature for 2 days. After the removal of DCM, the residue was washed with petroleum ether (2 × 5 mL) to remove unreacted tetraethyl vinylidene bisphosphonate and the pure product (PAA-BP) was obtained as a yellowish solid in 75% yield.

2.4. Acid-base titration

50 mg of each macromer was dissolved in deionized water with a concentration of 1 mg mL^{-1}. pH of the solution was first adjusted to 2.5 by use of 1 M HCl, and then the solution was titrated against 0.1 M NaOH with increments of 50 μL. The increase in pH was recorded with a pH meter (WTW Inolab pH 720) at room temperature.

2.5. Hydrogel preparation

PAA-NHBoc, PAA-NH_2 or PAA-BP crosslinked HEMA hydrogels were prepared by dissolving macromers (100 mg) and HEMA (900 mg) at the 10:90 wt% ratio in 3 mL distilled water. The photoinitiator (Irgacure 2959) (2 wt% of total monomer weight) was added and the mixture was placed into 2 mL syringes with inner diameter 4 mm. Then, the mixtures were exposed to UV light (365 nm) for 30 min in a photoreactor (Kerman UV/18) containing 12 Philips TL 8 W BLB lamps. The hydrogel samples were cut into pieces of length: 7 mm, thawed at room temperature, lyophilized and weighed (W_i). Then, unreacted gel precursors were removed by washing with ethanol (12 h) and distilled water (12 h), lyophilized and weighed again (W_f). The percent gelations were calculated according to Eq. (1):

$$Gelation\ (\%) = \frac{W_f}{W_i} \times 100 \quad (1)$$

2.6. Swelling studies

Swelling ratios of dry hydrogel samples (45 mg ± 5 mg) (W_d) were studied by immersing them in water, 0.5 M $CaCl_2$ solution and PBS (7.4 and 3) solutions at 37 °C to reach equilibrium swelling. The hydrogel samples were removed from the solutions, the excess solution was removed with tissue paper and the swollen weight (W_s) was measured.

The degree of swelling (D_s) was calculated using the following Eq. (2):

$$D_s = \frac{W_s - W_d}{W_d} \times 100 \quad (2)$$

where W_s and W_d refer to the weight of swollen and dry gel samples, respectively. The average data obtained from triplicate measurements were reported.

2.7. Degradation studies

In vitro degradation studies of the hydrogels were conducted by immersing dry hydrogel samples (45 mg ± 5 mg) (W_i) in PBS solution (5 mL) at 37 °C and pH 7.4. At predetermined time intervals (1, 2 and 4 weeks) samples were taken out, rinsed with water, freeze-dried and re-weighed (W_f). The measurements were made in triplicate and the average data were reported. The degradation % was calculated according to Eq. (3):

$$Degradation\ (\%) = \frac{W_i - W_f}{W_i} \times 100 \quad (3)$$

2.8. Water contact angle measurements

Freeze-dried hydrogel samples were allowed to swell in water and then air-dried at 25 °C. To obtain flat surfaced hydrogels at their semi-dried state, hydrogels were placed between two glass slides and allowed to dry further. Water contact angle values of hydrogels were measured in air via the sessile-drop method using a goniometer (CAM 101 KSV instruments). The side profiles of deionized water drops (approximately 3–5 μL) were recorded by an integrated digital camera for image analysis. The dynamic contact angle values were measured by the shape of the drop recorded in a time range of 0–10 s, collecting images every 1 s. Every contact angle value of the hydrogel was determined at five different spots on the sample and average contact angle values were reported.

2.9. Mineralization of the hydrogels

Hydrogel samples were immersed into 5 times concentrated simulated body fluid (5xSBF) solution, prepared as described by Chou et al [47], and incubated at 37 °C for two days during which 5xSBF was changed every day. Then hydrogels were taken out of the solution, kept overnight in deionized water and freeze-dried to constant weight. The characterization of mineralized hydrogels was carried out by using TGA, FTIR, SEM, EDX and XRD analyses.

2.10. Mechanical studies

Mechanical properties of hydrogels in equilibrium swollen states in water were investigated by uniaxial compression measurements on a Zwick Roell test machine with a 500 N load cell in a thermostated room at 25 °C. The tests were carried out at a constant cross-head speed of 5 mm min^{-1}. Before the tests, a complete contact between the gel specimen and the metal plate was provided by applying an initial compressive force of 0.05 N. The compressive stress is calculated as its nominal σ_{nom}, which is the force per cross-sectional area of the undeformed gel specimen, while strain is given by ε which is the change in the specimen length with respect to its initial length. Young's modulus E of the hydrogels was calculated from the slope of stress–strain curves between 5 and 15% compressions. Measurements were made with at least 3 hydrogels and the results were averaged.

2.11. In vitro cytotoxicity assay

Impact of the degradation products of the prepared gels on the viability of Saos-2, U-2 OS, NIH 3T3 and C2C12 cell lines was evaluated using the standard MTT assay. The NIH 3T3 and U-2 OS cells were cultured in phenol red containing DMEM complete medium, and C2C12 cells were cultured in DMEM without containing phenol red, supplemented with 10% (v/v) FBS and 1% (v/v) pen-strep in a 5% CO_2-humidified incubator at 37 °C and passaged every 2–3 days. Saos-2 cells were cultured in the same way using McCoy 5A complete medium. For viability test, cells were seeded at a density of 37.5×10^3 cells/mL for C2C12 cells and 75×10^3 cells/mL for other cells in each well of a 96-well plate and incubated at 37 °C in 5% CO_2 atmosphere. The degradation product was added at a concentration between 5 and 100 μg/mL. After 48 h incubation, the cell viability was assessed using MTT colorimetric assay. First, 50 μL of MTT solution (5 mg/mL in PBS) was added into each well with 150 μL of culture medium and incubated for 4 h. Then, the purple formazan crystals formed as a result of mitochondrial activity in viable cells were dissolved with ethanol: dimethyl sulfoxide (1:1 v/v) mixture. Absorbance at 570 nm with a reference reading at 630 nm was recorded for each well using a Synergy – H1 microplate reader (BioTek Instruments Inc., Winooski, VT, USA). Cells which were not exposed to degradation products of gels were used as controls which were assumed as 100% viability. The relative cell viability was calculated by using following Eq. (4):

$$Cell\ viability\ (\%) = \frac{Absorbance\ (Sample)}{Absorbance\ (Control)} \times 100 \quad (4)$$

2.12. Cell attachment experiment

To investigate cell interaction of the mineralized hydrogels, PAA-BP crosslinked HEMA hydrogels were prepared as described in Section 2.5 on treated polystyrene 48-well plates. 5xSBF was added onto the hydrogel samples to initiate mineralization and the plates were kept at 37 °C for two days during which 5xSBF was changed every 12 h. The

mineralized hydrogels were washed with PBS and sterilized under UV light. Then, C2C12 cells at a density of 66.7 × 10^3 cells/mL in complete medium were seeded to 48 well plate and incubated for 20 h. After washing twice with PBS, cells were fixed with 4% paraformaldehyde solution for 20 min and washed again twice with PBS. Cells were stained with DAPI and phalloidin solution (both 4 μg/mL in PBS) for 20 min, washed twice with PBS and stored at 4 °C in 0.2 mL PBS to prevent the cells from drying out. Then, the fixed cells were visualized under Zeiss Axio Observer Z1 Fluorescence Microscope (Germany) equipped with DAPI filter for nucleus staining and FTIC filter for cytoskeleton staining with phalloidin. Images were colored and merged using the ZEN 3.1 (Blue version) software.

3. Results and discussion

3.1. Synthesis and characterization of PAA Macromers

A novel bisphosphonate-functionalized PAA macromer (PAA-BP) was synthesized in three steps as shown in Fig. 1. The first step involves aza-Michael reaction of MBA and *N*-Boc-1,6-hexanediamine (1.2:1 bisacrylamide to amine mol ratio) at 50 °C for 4 days in methanol:water (1/3 v/v), mixture. A macromer (PAA-NHBoc) with the *N-tert*-butyloxycarbonyl (*N*-Boc)-protected amine group in the side chain was obtained as a white solid in 90% yield. This macromer was used as a control macromer to examine the effect of BP functionality on mineralization properties of the hydrogels. In the second step, the selective deprotection of the *N*-Boc group was performed by acidic cleavage using TFA to obtain a macromer (PAA-NH_2) in its CF_3COOH-salt form. In the literature, linear polymer of the same macromer with the pendant primary amine HCl salt was synthesized by Michael polyaddition of the bisacylamide and protected amine in 1:1 mol ratio without solvent at 140 °C for about 12 h, followed by deprotection using HCl [48]. In another study, the deprotection of the amino groups of bioreducible PAAs with oligoamine side chains was carried out in a mixture of methanol/TFA and HCl for 4–6 h [49]. The deprotonation of the ammonium groups to neutral primary amines was performed using sodium hydroxide solution to give PAA-NH_2 as a white solid in 80% yield. This macromer was also used as a control macromer to compare the effect of BP and NH_2 functionality on hydrogel properties such as mineralization. In the third step, post-modification of primary amines on the macromer was carried out: PAA-NH_2 was reacted with excess amount of tetraethyl vinylidene bisphosphonate by aza-Michael addition to give the novel macromer (PAA-BP) with side chain bisphosphonate groups, as a yellowish solid in 75% yield. PAA-NH_2 and PAA-BP showed good solubility in water.

The chemical structure of the macromers synthesized in each reaction step was verified by the ^{1}H NMR spectroscopy and FTIR (Fig. 2 and Fig. 3). ^{1}H NMR of the product of the first step shows Boc groups at 1.36 ppm, acrylamide end groups at 5.62 and 6.19 ppm and methylene protons of MBA at 4.49 ppm. The number of repeating unit (*n*) of this macromer was calculated by the ratio of the integrals of acrylamide double bond protons to the Boc protons and found to be 11. From the number of repeating units, the number-average molecular weight was calculated using M_n = (FW end groups) + (FW repeating unit)(*n*) as 4250 g/mol. After the second step, no peak was present around 1.36 ppm, corresponding to Boc group, indicating that the deprotection is complete. Also, we observe a downfield shift of most of the peaks (except k, i, h). This effect is due to decreased shielding of the protons due to positively charged ammonium ions relative to neutral amine. ^{13}C NMR spectrum of this product also confirmed its structure (Fig. S1). The M_n of this PAA macromer (PAA-NH_2) was calculated as 3150 g/mol. In the last step, ethyl protons of bisphosphonate group showed two splitted peaks at 4.24 and 1.39 ppm in ^{1}H NMR spectrum due to the coupling of the phosphorus signals to the protons in the compound. The average degree of substitution of the bisphosphonate group, determined from the ^{1}H NMR spectrum by integrating bisphosphonate protons z or n with respect to double bond peaks (k, i), was found to be 50%, although excess amount of tetraethyl vinylidene bisphosphonate was used. This may be explained by the fact that BP groups are bulky groups, they cause steric hindrance as they are added to the structure. Also because BP functionalization occurs via Michael addition reaction, *retro*-Michael reaction could occur, decreasing the degree of substitution [50]. Although this macromer was abbreviated as PAA-BP it has a copolymeric structure, having 50% of PAA-NH_2 units. M_n value of this macromer was calculated as 4800 g/mol.

The FTIR spectra of PAA-NH_2 and PAA-BP show broad peaks in the region of 3500–3150 cm^{-1} due to NH stretching and strong peaks at 1712 cm^{-1} because of C═O stretching (Fig. 3A). Moreover, the strong bands at 1017 and 980 cm^{-1} in the FTIR spectra of PAA-BP correspond to the symmetric and asymmetric vibration of P—O, which are absent in PAA-NH_2 spectrum.

The pH sensitivities of PAA-NH_2 and PAA-BP macromers were evaluated by acid-base titration (Fig. 3B). For both macromers a plateau region was observed in the pH range of about 6–8, which is characteristic for poly(amido amine)s [48,51].The plateau is wider for PAA-BP compared to PAA-NH_2, indicating its better pH-responsive

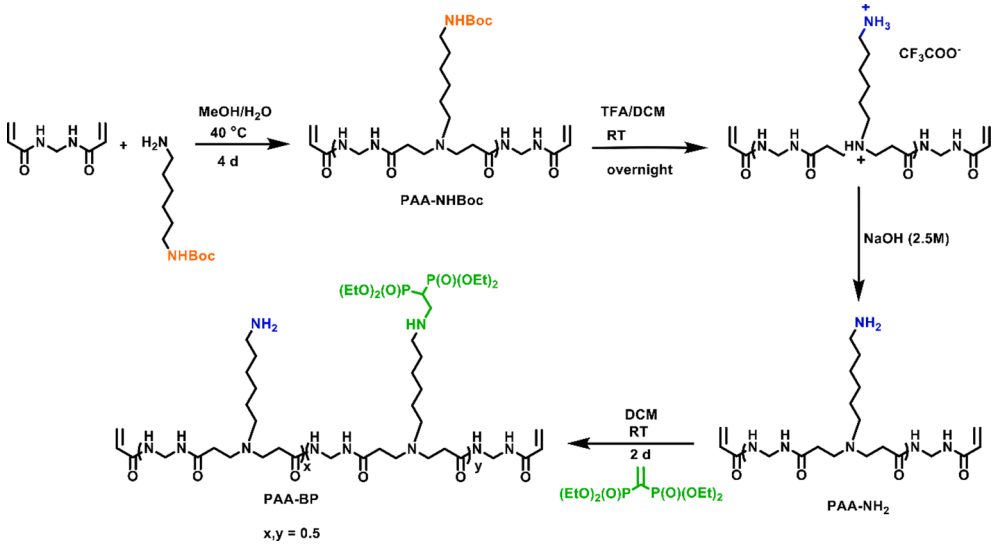

Fig. 1. Synthesis of poly(amido amine) macromer with BP side chains.

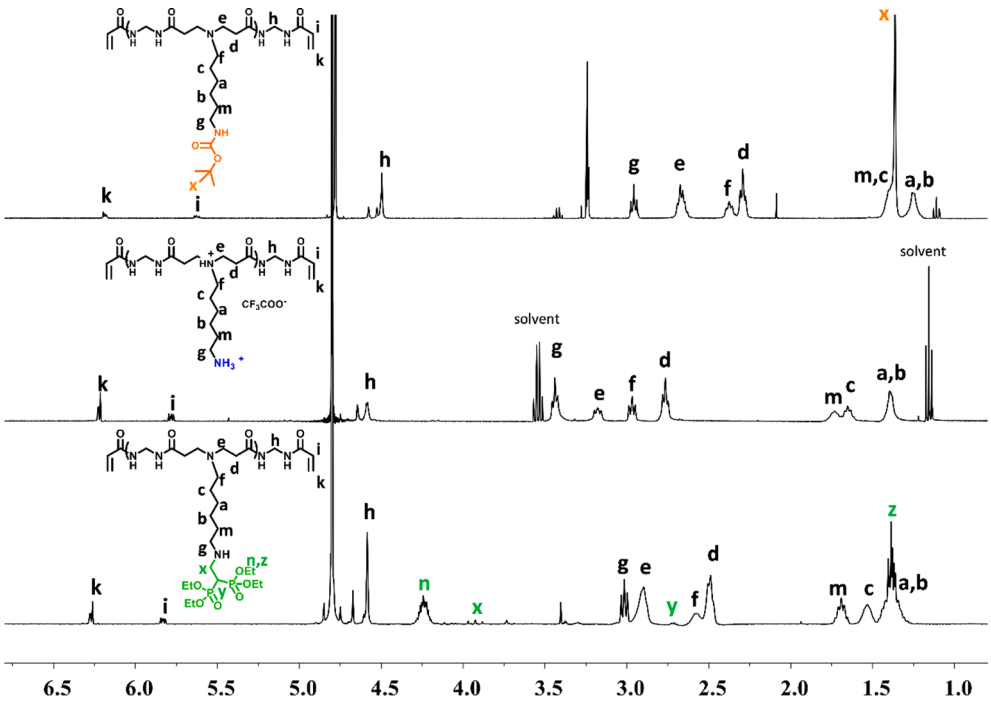

Fig. 2. ^{1}H NMR spectra of products of each reaction step during synthesis of PAA-BP.

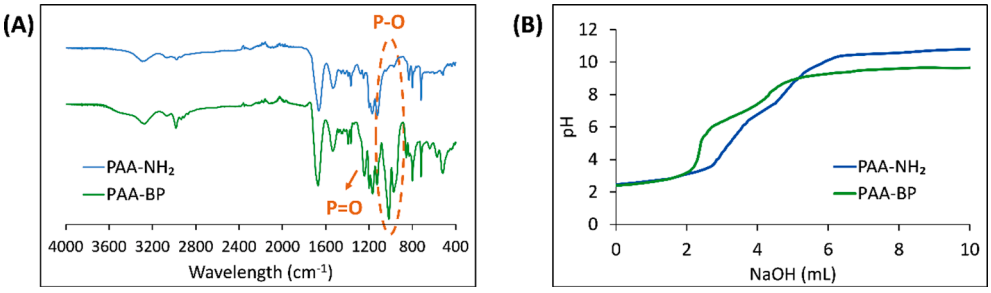

Fig. 3. (A) FTIR spectra and (B) acid-base titration curves of PAA-NH_2 and PAA-BP macromers.

performance. PAA-NH_2 with higher hydrophilicity at low pH deprotonates continuously with an increase in pH, thus it does not show as distinct a plateau as PAA-BP.

The thermal properties of the PAA-NH_2 and PAA-BP macromers investigated by DSC showed their glass transition temperatures (T_g) as 27 °C and 38 °C (Fig. S2). The higher T_g value of PAA-BP can be explained by the steric hindrance of bulky BP groups and their polar interaction.

3.2. Synthesis and characterization of hydrogels

To understand the effect of the bisphosphonate group on hydrogel properties, two of the macromers (PAA-NH_2 and PAA-BP) (10 wt%) were copolymerized with HEMA (90 wt%) by free radical photopolymerization using Irgacure 2959 as photoinitiator (Fig. 4). The hydrogels are named as H:PAA-NH_2 and H:PAA-BP where "H" stands for hydrogel and PAA-x indicates the crosslinker. Gelation percentages of the hydrogels were found as 80 and 85% for PAA-NH_2 and PAA-BP, respectively.

SEM micrographs of synthesized hydrogels showed that hydrogels have macroporous (pore size > 100 μm) morphology which is one of the essential requirement for the tissue engineering scaffolds and directly affects bone formation (Fig. 5A) [52]. The pore size of hydrogels were found as around 170 μm for H:PAA-NH_2 and 275 μm for H:PAA-BP

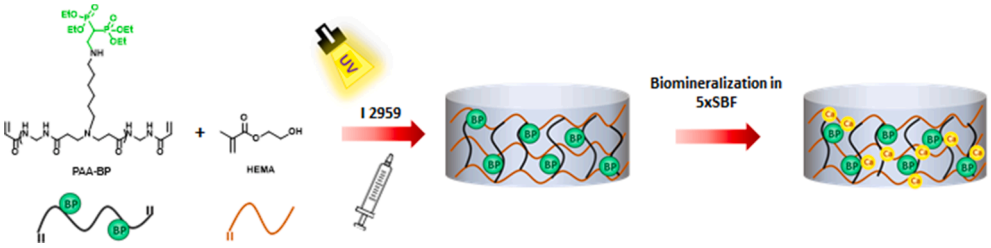

Fig. 4. The preparation of H:PAA-BP and its biomineralization in 5xSBF.

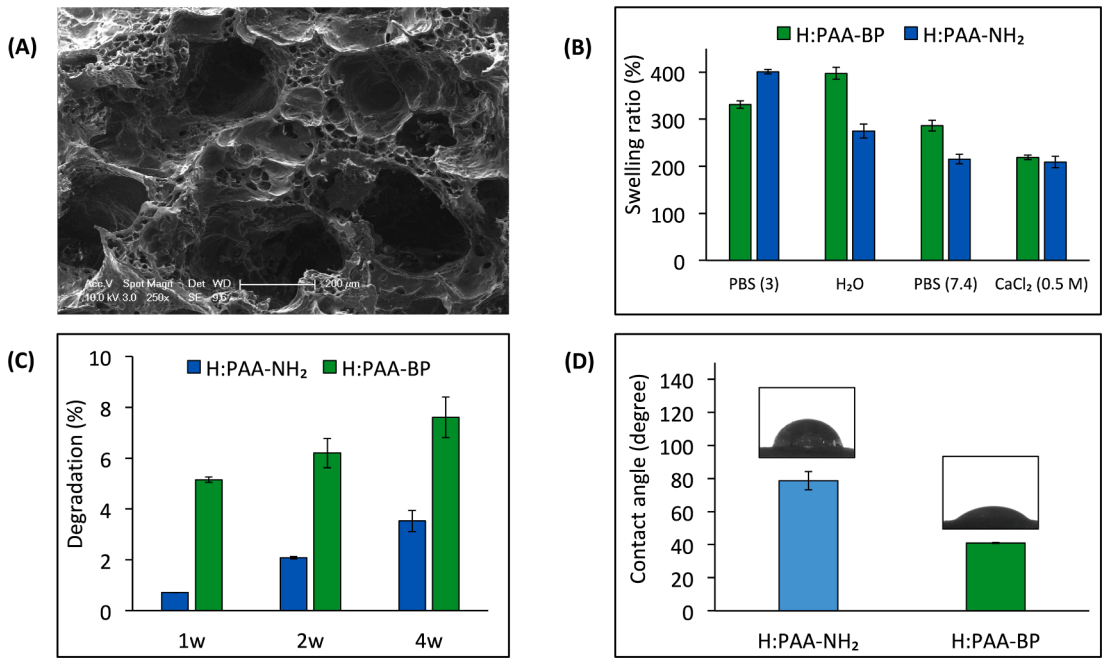

Fig. 5. (A) SEM image of H:PAA-BP, (B) equilibrium swelling ratio (%) of hydrogels in water, various buffer and $CaCl_2$ solutions, (C) degradation (%) of hydrogels in PBS (pH 7.4) solution at 37 °C and (D) water contact angles of the hydrogels.

(Fig. S3). This difference can be explained by different crosslink density and/or hydrophilicity of the crosslinkers. H:PAA-BP hydrogel with lower mol% of crosslinker (since hydrogels are prepared by using same weight percentages of crosslinkers having different molecular weights) is expected to have lower crosslinking density than that of H:PAA-NH_2. Besides, the more hydrophilic crosslinker PAA-BP may also increase the pore size.

3.3. Swelling, degradation and wettability behaviour

In general, the structural properties of hydrogels such as the hydrophilic/hydrophobic balance, the degree of cross-linking and the degree of ionization are the important parameters which control the equilibrium swelling. The swelling ratios of the synthesized hydrogel samples with two different PAA crosslinkers, PAA-BP and PAA-NH_2, in distilled water, $CaCl_2$ solution (0.5 M) and buffer solutions (pH 3.0 and 7.4) are shown in Fig. 5B. It was observed that after 120 min equilibrium swelling was reached in all solutions. The swelling capacity of the PAA-BP crosslinked hydrogels was found to be higher than those of the PAA-NH_2 crosslinked ones in water and in pH 7.4. This can be explained by two factors: i) lower crosslink density (as explained above) and ii) the more hydrophilic nature of PAA-BP due to pendant secondary amine groups and BP groups: The pendant secondary groups may be already protonated at pH 7.4 and water in addition to tertiary amine ($pK_a = 6–8$) groups at the backbone. The protonated amines cause more electrostatic repulsion between chains and lead to the expansion of the network, hence diffusion of water into the network. However the NH_2 groups on the H:PAA-NH_2 hydrogel are not protonated at neutral pH because the pK_a value of the pendant primary amine group is approximately 6.5 [53] and stronger hydrogen bonding ability of these groups compared to in H:PAA-BP causes more crosslinking sites and therefore more compact structure. The swelling ratios of both hydrogels were found to be lower at pH 7.4 than in water, indicating high ion concentration preventing electrostatic repulsion which is more effective in PAA-BP crosslinked hydrogels.

The effect of acidic pH on the swelling ratios of the hydrogels is also measured at pH 3.0 and illustrated in Fig. 5B. The hydrogels showed different swelling behaviors in acidic solutions. It can be seen that the swelling ratio of H:PAA-NH_2 increased with decreasing the pH. The NH_2 groups on the hydrogel are protonated at acidic pH, the electrostatic repulsion causes breaking of hydrogen bonding between the chains, leading to the expansion of the network. We also expected an increase in swelling ratio of H:PAA-BP due to protonation of NH_2 groups in its structure. However, we observed a decrease compared to those of H:PAA-NH_2. This unexpected behavior can be explained by the presence of ionic groups at the side chain of PAA-BP crosslinker under neutral conditions which decrease the effect of hydrogen bonding due to NH_2 groups. Therefore increase in ion concentration at low pH decreases the electrostatic repulsion already present in neutral form and thus swelling decreases compared to in water.

The swelling ratios of both hydrogels decreased in $CaCl_2$ solution compared to in water, more so for H:PAA-BP than for H:PAA-NH_2 (Fig. 5B) which indicates interaction of BP groups with Ca^{2+} ions forming physical crosslinking.

The degradation behavior of the hydrogels was investigated in PBS (pH 7.4) at 37 °C (Fig. 5C). The mass loss of the gels was found to change between 1 and 8% in four weeks, the main reason for the difference being differences in chemical structure such as hydrophilicity (coming from PAA-BP), the extent of secondary interactions (hydrogen bonding between NH_2 groups) and crosslink density. While H:PAA-BP hydrogels showed higher mass loss, H:PAA-NH_2 hydrogels which do not possess BP groups and have higher crosslink density showed lower degradation rate.

The contact angle of water droplet on the gel surface was determined using static water contact angle measurement at ambient temperature. The contact angle decreased from 79° (H:PAA-NH_2) to 41° (H:PAA-BP) with the increasing hydrophilicity arising from the PAA-BP crosslinker (Fig. 5D).

3.4. Mineralization of hydrogels

The ability of materials to form calcium phosphate (CaP) phases at their surface similar to bone mineral is tested by immersing them in SBF, which mimics the ionic concentrations and pH typically observed in plasma. In the literature, the different types of SBF solutions have been developed with varying compositions [54]. In this study, we used high

SBF concentrations (5xSBF) in order to increase the rate of biomimetic mineralization. In order to assess the role of NH_2 and NH_2/BP functional groups in the mineralization properties of the synthesized hydrogels, a H:PAA-NHBoc hydrogel was also prepared and used as control. After hydrogels (H:PAA-NHBoc, H:PAA-NH_2 and H:PAA-BP) were immersed in 5xSBF for 2 days and washed with deionized water overnight, they were freeze-dried. CaP minerals deposited were characterized by SEM, EDX, XRD, FTIR and TGA.

The FTIR spectra of all the hydrogels before mineralization mainly show absorption peaks of HEMA due to its high concentration, the broad OH stretching peak at around 3400 cm^{-1} and the C═O stretching at 1712 cm^{-1} (Fig. 6A). The FTIR spectra obtained for mineralized H:PAA-NHBoc, H:PAA-NH_2 and H:PAA-BP hydrogels were used to characterize mineral phases in the samples (Fig. 6B). As is known, there are four Raman and IR active vibrational modes for phosphate ions. O—P—O bending vibrations were indicated by the very intense ν_3PO mode between 1190 and 976 cm^{-1} and ν_4PO mode between 660 and 520 cm^{-1}. Also, phosphate ν_1PO band is observed at 962 cm^{-1} and ν_2PO band is observed in the region of 475 and 440 cm^{-1} as weak bands [55]. The spectra of mineralized H:PAA-NH_2 and H:PAA-BP are dominated by these peaks, similar to HAP. These observations, together with a significant decrease (complete disappearance for H:PAA-BP) in polymer peaks indicates a large amount of mineral on H:PAA-NH_2 and H:PAA-BP hydrogels. However, no major change in spectrum of H:PAA-NHBoc was observed, indicating that mineralization is not occurring. Furthermore, the mineralization performance of H:PAA-NH_2 can be explained by the fact that polycations such as linear PEI also have a strong effect on CaP mineralization [56].

Formation of mineral phase was also confirmed by scanning electron microscopic (SEM) analysis of mineralized and freeze-dried hydrogels H:PAA-NH_2 and H:PAA-BP. Both showed needle-like crystals similar to HAP covering their whole surface when immersed in 5xSBF (Fig. 7A and B). However, at one order of magnitude larger scale H:PAA-BP features are more or less uniform, but for H:PAA-NH_2 the needles occasionally aggregate into roughly spherical particles on the calcium phosphate layer. EDX was used to investigate the element composition of the inorganic complex and showed the presence of C, O, P, Ca and Mg in the mineralized samples (Fig. 7A and B). The Ca/P ratios was found to be 1.5 for both hydrogels. This ratio is known to be 1.67, 1.5, 1.0 and 1.33 in HAP [$Ca_{10}(PO_4)_6(OH)_2$], calcium phosphate [$Ca_3(PO_4)_2$] (amorphous), brushite [$(CaHPO_4)_3$-H_2O], and octacalcium phosphate [$Ca_8(PO_4)_6H_2$] [15,57]. These results suggest the formation of an apatite-like mineral, nonstoichiometric HAP.

The crystal properties of the deposited minerals were analyzed by XRD measurements. In general, two XRD reflection peaks are used to monitor the HAP formation; one at $2\theta = 26$ and the other group is ranging from $2\theta = 30$ to $2\theta = 34$–36 [58,59]. We also observed peaks at about $2\theta = 26$ and $2\theta = 32°$ indicating apatitic minerals (Fig. 8A).

The TGA thermograms which indicate the degree of mineralization were investigated for H:PAA-BP hydrogel before and after mineralization and compared with the mineralization of H:PAA-NH_2 hydrogel (Fig. 8B). For all hydrogels the first weight loss at ca. 100 °C is due to dehydration processes. The unmineralized H:PAA-BP hydrogel started to degrade at ca. 200 °C, whereas for the mineralized ones this temperature was shifted to ca. 300 °C probably due higher thermal stability of the hybrid materials. The weight loss continued until ca. 500 °C due to degradation of the main chain. The final amount of inorganics are 23 and 12% for H:PAA-BP and H:PAA-NH_2 hydrogels, compared to 0.9% for unmineralized H:PAA-BP hydrogel. This indicates that both the BP and amine groups contribute to mineralization but the performance of the former is better.

3.5. Mechanical properties

Mechanical properties of the gels in their equilibrium swollen states were investigated by uniaxial compression tests. Fig. 9 shows nominal stress (σ_{nom})–strain (ε) curves and Young's modulus E of hydrogels before and after mineralization in 5xSBF. It is seen that both Young's modulus E and compressive strength of the BP containing hydrogel (H:PAA-BP) is higher than that of the control hydrogel (H:PAA-NH_2). For example, the modulus E of the H:PAA-BP hydrogel is 42 ± 2 kPa compared to H:PAA-NH_2 hydrogel with a value of 34 ± 2 kPa. Mechanical tests were also conducted on mineralized hydrogels. It was observed that mineralization significantly affects the mechanical performances of both hydrogels, the modulus E increasing from 34 ± 2 kPa to 54 ± 3 kPa for H:PAA-NH_2 hydrogel and from 42 ± 2 kPa to 83 ± 1 kPa for the H:PAA-BP hydrogel. As expected, higher increase on mechanical properties was seen for the BP containing H:PAA-BP hydrogel after mineralization due to the physical interaction between polymer and HAP like minerals forming on hydrogels.

3.6. In vitro cytotoxicity of hydrogel degradation products

Cytocompatibility of hydrogels was determined by extracting degradation products from the hydrogels and then exposing Saos-2, U-2 OS, NIH 3 T3 and C2C12 cells to the extracts. A cell type and dose-dependent (5–100 μg/ml) study was performed in order to evaluate the influence of concentration of the degradation products as well as their composition on the viability of the cell lines (Fig. 10). Cell viability above 80% is assumed as noncytotoxic according to ISO 10993–5 [60]. It was observed that both hydrogels' degradation products did not cause significant cytotoxicity in osteosarcoma cells (Saos-2 and U-2 OS cells) and muscle cells (C2C12 cells); and a low cytotoxicity (75% viability) of the degradation products of the control hydrogel was detected for NIH 3T3 cells at the highest tested concentration, 100 μg/ml due to more vulnerable nature of these cells.

3.7. Cell interaction studies

The ability to support cell proliferation is an essential requirement for tissue engineering scaffolds. Bisphosphonic acid, phosphate and phosphonic acid functional groups are known to positively affect cell adhesion, proliferation and spread [61–63]. Likewise, mineralized HAP or similar mineral layers on the gel layer leads to improved cell viability

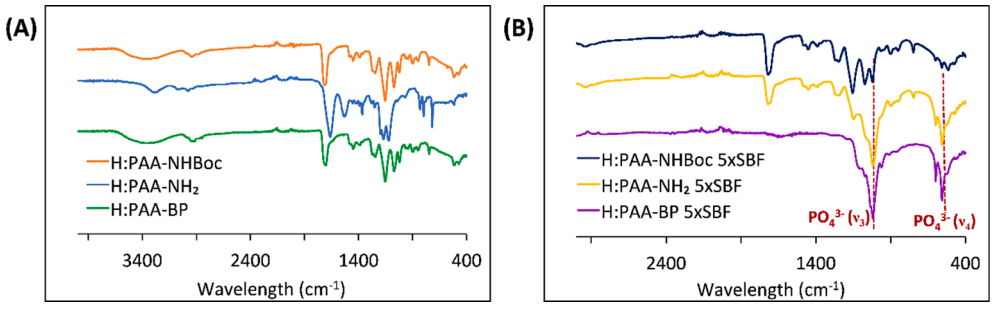

Fig. 6. FTIR spectra of hydrogels (A) before and (B) after mineralization in in 5xSBF.

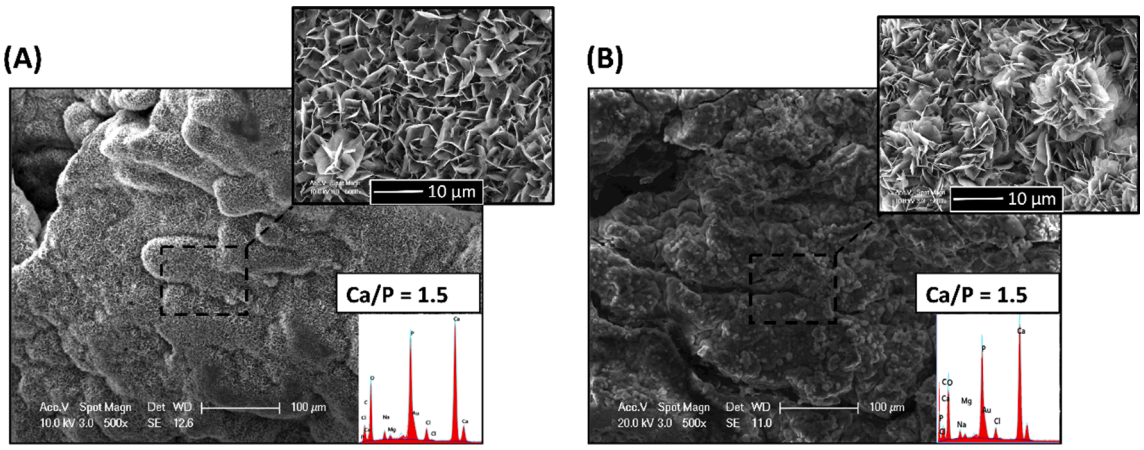

Fig. 7. SEM images and EDX spectra (inset) of hydrogels (A) H:PAA-BP and (B) H:PAA-NH_2, mineralized by immersion in 5xSBF.

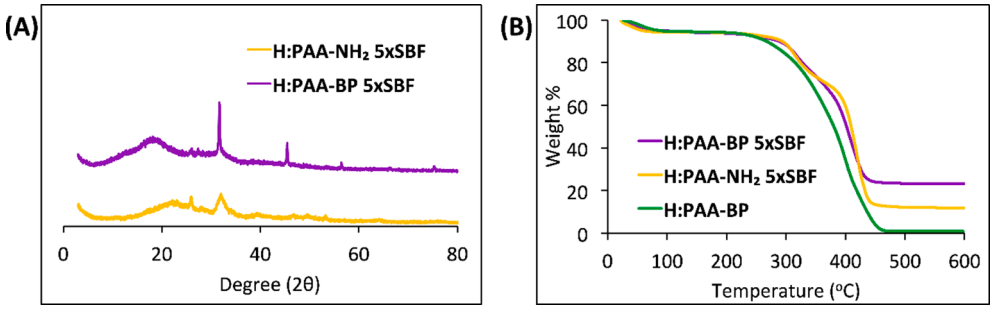

Fig. 8. (A) XRD spectra for hydrogels H:PAA-BP and H:PAA-NH_2 before and after mineralization in 5xSBF, (B) TGA thermograms of H:PAA-BP, before and after mineralization, and H:PAA-NH_2 after mineralization, in 5xSBF.

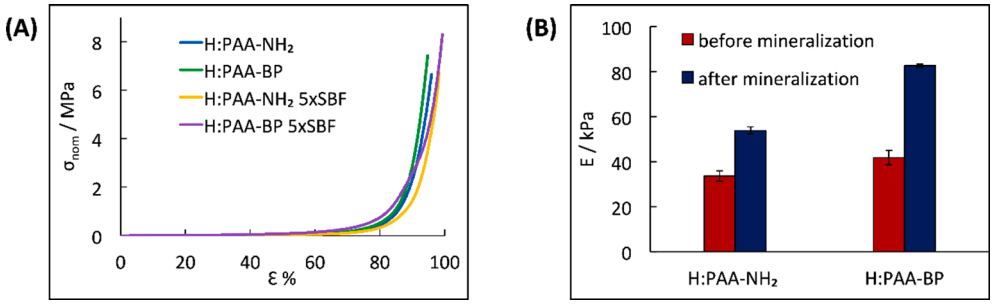

Fig. 9. Stress – strain curves (A) and Young's modulus E (B) of H:PAA-NH_2 and H:PAA-BP before and after mineralization in 5xSBF.

[64,65]. Here, we also observed successful attachment of C2C12 mouse myoblast muscle cells on mineralized H:PAA-BP hydrogels. Fluorescence images (Fig. 11) obtained from cells stained with nuclear stain DAPI (blue) and cytoskeleton stain phalloidin (Green) show that attachment, spread, density, and the health of cells on mineralized hydrogels are comparable to those seen in control cells which were directly seeded on culture plates. Cytoskeleton staining with phalloidin (Green) interacted with the gel but still shows the cytoskeleton around nuclei. These suggest that mineralized gels are suitable for attachment and proliferation of cells with no specific toxicity.

4. Conclusions

A HEMA-based hydrogel bearing BP groups was shown to be an effective biomaterial for biomineralization. The hydrogel was synthesized by copolymerization of HEMA and a PAA macromer, where BP groups were incorporated into about half of the primary amine groups present at the side chains of the macromer in the previous step of the synthesis. This novel hydrogel was compared with one produced from the PAA macromer with no BP functionalization, i.e. featuring NH_2 only (control hydrogel). The macromers were found to enhance degradability of HEMA hydrogels (H:PAA-BP and H:PAA-NH_2), controlled by their hydrophilicity and hydrogen bonding interactions due to BP and NH_2 groups. The equilibrium swelling of both hydrogels were highly sensitive to pH of the swelling medium. In addition, H:PAA-BP's swelling is also positively affected by the presence of $CaCl_2$, which indicates the formation of physical crosslinks between BP groups and Ca^{2+} ions. Both hydrogels showed HAP like mineral layers in 5xSBF, with mineral contents of 23 and 12% for H:PAA-BP and H:PAA-NH_2 hydrogels respectively, indicating better performance of the former. These results show that for purposes of adding mineralization ability to hydrogel biomaterials, the BP groups constitute an alternative to the bisphosphonic acid groups previously investigated in the literature. The mineralization significantly affects the mechanical performances of both

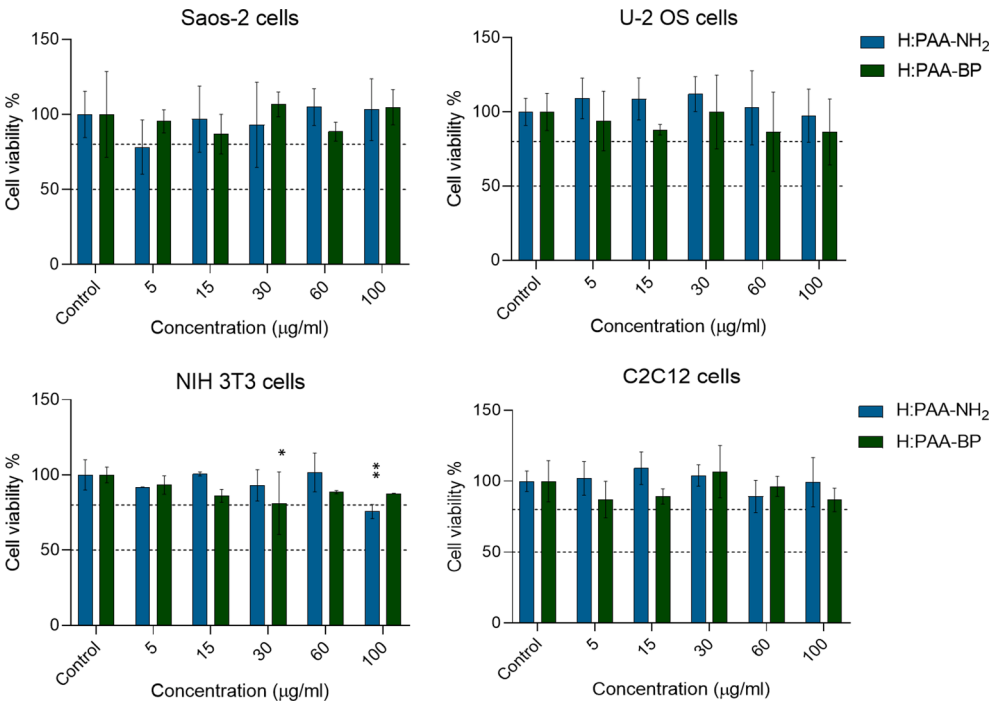

Fig. 10. Viability of Saos-2, U-2 OS, NIH 3T3 and C2C12 cell lines treated with degradation products of H:PAA-NH_2 and H:PAA-BP for 48 h. Statistics were conducted by using an ordinary one-way ANOVA analysis of variance followed by multiple Dunnett's comparison test of GraphPad Prism 8 software. Data were presented as mean ± SD of independent experiments (n = 6 for Saos-2, U-2 OS and C2C12 cells, n = 4 for NIH 3 T3 cells). $p < 0.05$ was accepted as a statistically significant difference. $p < 0.0332$(*) and $p < 0.0021$(**). Dashed lines show the 80% and 50% viability.

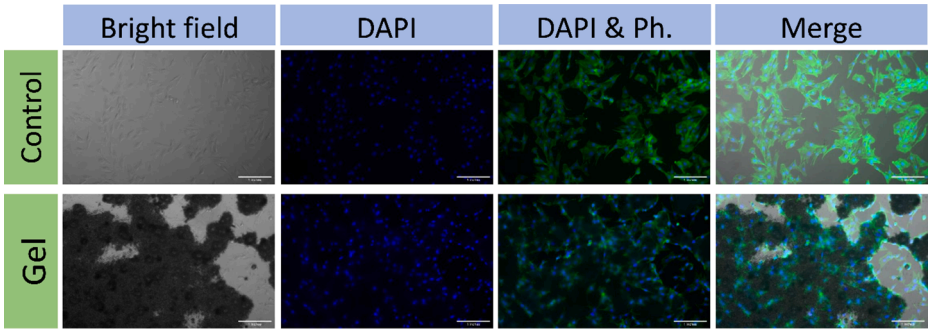

Fig. 11. Attachment and spread of C2C12 myoblast muscle cells on the mineralized H-PAA-BP gel after 20 h of incubation. Blue: Nuclear DAPI stain; Green: Phalloidin cytoskeleton stain. Filters: DAPI filter and FITC filter. Magnification: 10×. Scale: 200 μm.

H:PAA-BP and H:PAA-NH_2 hydrogels, as expected PAA-BP forming stronger hydrogel-apatite composites compared to PAA-NH_2. The cell experiments showed that H:PAA-BP hydrogel facilitates cell attachment, spread and proliferation after mineralization. Therefore these materials, especially the novel H:PAA-BP hydrogel, have great potential for use in tissue engineering applications.

CRediT authorship contribution statement

Melek Naz Guven: Investigation, Writing – original draft. **Burcu Balaban:** Investigation. **Gozde Demirci:** Investigation. **Havva Yagci Acar:** Resources, Supervision, Writing – review & editing. **Oguz Okay:** Resources, Supervision. **Duygu Avci:** Conceptualization, Supervision, Resources, Writing – review & editing, Project administration.

Declaration of Competing Interest

The authors declare that they have no known competing financial interests or personal relationships that could have appeared to influence the work reported in this paper.

Acknowledgments

This work was financed by TUBITAK grant number 117Z330.

The raw/processed data required to reproduce these findings cannot be shared at this time due to technical or time limitations.

Appendix A. Supplementary material

Supplementary data to this article can be found online at https://doi.org/10.1016/j.eurpolymj.2021.110732.

References

[1] G.L. Koons, M. Diba, A.G. Mikos, Materials design for bone-tissue engineering, Nat. Rev. Mater. 5 (8) (2020) 584–603.
[2] L. Shi, P. Ding, Y. Wang, Y. Zhang, D. Ossipov, J. Hilborn, Self-healing polymeric hydrogel formed by metal–ligand coordination assembly: Design, fabrication, and biomedical applications, Macromol. Rapid Commun. 40 (2019) 1800837.
[3] C.M. Agrawal, R.B. Ray, Biodegradable polymeric scaffolds for musculoskeletal tissue engineering, J. Biomed. Mater. Res. 55 (2) (2001) 141–150.
[4] D.W. Hutmacher, Scaffolds in tissue engineering bone and cartilage, Biomaterials 21 (24) (2000) 2529–2543.
[5] M.I. Sabir, X. Xu, L.i. Li, A review on biodegradable polymeric materials for bone tissue engineering applications, J. Mater. Sci. 44 (21) (2009) 5713–5724.

[6] A.S. Hoffman, Hydrogels for biomedical applications, Adv. Drug Deliv. Rev. 64 (2012) 18–23.
[7] C.d.L.H. Alarcón, S. Pennadam, C. Alexander, Stimuli responsive polymers for biomedical applications, Chem. Soc. Rev. 34 (3) (2005) 276–285.
[8] S. Mantha, S. Pillai, P. Khayambashi, A. Upadhyay, Y. Zhang, O. Tao, H.M. Pham, S.D. Tran, Smart hydrogels in tissue engineering and regenerative medicine, Materials 12 (20) (2019) 3323, https://doi.org/10.3390/ma12203323.
[9] J.L. Drury, D.J. Mooney, Hydrogels for tissue engineering: scaffold design variables and applications, Biomaterials 24 (24) (2003) 4337–4351.
[10] E. Calo, V.V. Khutoryanskiy, Biomedical applications of hydrogels: A review of patents and commercial products, Eur. Polym. J. 65 (2015) 252–267.
[11] D. Puppi, C. Migone, A. Morelli, C. Bartoli, M. Gazzarri, D. Pasini, F. Chiellini, Microstructured chitosan/ poly(γ-glutamic acid) polyelectrolyte complex hydrogels by computer-aided wet-spinning for biomedical three-dimensional scaffolds, J. Bioact. Compat. Polym. 31 (2016) 531–549.
[12] C.L. Zaccaria, V. Cedrati, A. Nitti, E. Chiesa, A. Martinez de Ilarduya, M. Garcia-Alvarez, M. Meli, G. Colombo, D. Pasini, Biocompatible graft copolymers from bacterial poly(γ-glutamic acid) and poly(lactic acid), Polym. Chem. 12 (26) (2021) 3784–3793.
[13] S. Van Vlierberghe, P. Dubruel, E. Schacht, Biopolymer-based hydrogels as scaffolds for tissue engineering applications: A review, Biomacromolecules 12 (5) (2011) 1387–1408.
[14] K. Gkioni, S.C.G. Leeuwenburgh, T.E.L. Douglas, A.G. Mikos, J.A. Jansen, Mineralization of hydrogels for bone regeneration, Tissue Eng. B Rev. 16 (6) (2010) 577–585.
[15] S. Suzuki, M.R. Whittaker, L. Grøndahl, M.J. Monteiro, E. Wentrup-Byrne, Synthesis of soluble phosphate polymers by RAFT and their in vitro mineralization, Biomacromolecules 7 (11) (2006) 3178–3187.
[16] T.V. Chirila, Zainuddin, D.J.T. Hill, A.K. Whittaker, A. Kemp, Kemp, Effect of phosphate functional groups on the calcification capacity of acrylic hydrogels, Acta Biomater. 3 (1) (2007) 95–102.
[17] C.W. Kim, S.E. Kim, Y.W. Kim, H.J. Lee, H.W. Choi, J.H. Chang, J. Choi, K.J. Kim, K.B. Shim, Y.-K. Jeong, S.C. Lee, Fabrication of hybrid composites based on biomineralization of phosphorylated poly(ethylene glycol) hydrogels, J. Mater. Res. 24 (1) (2009) 50–57.
[18] X. Yang, S. Akhtar, S. Rubino, K. Leifer, J. Hilborn, D. Ossipov, Direct ″click″ synthesis of hybrid bisphosphonate–hyaluronic acid hydrogel in aqueous solution for biomineralization, Chem. Mater. 24 (9) (2012) 1690–1697.
[19] E. Boanini, M. Gazzano, K. Rubini, A. Bigi, Composite nanocrystals provide new insight on alendronate interaction with hydroxyapatite structure, Adv. Mater. 19 (18) (2007) 2499–2502.
[20] M.N. Guven, G. Demirci, S. Altuncu, U. Gulyuz, O. Okay, H.Y. Acar, D. Avci, Alendronate-functionalized poly(amido amine) cryogels of high-toughness for biomedical applications, Polymer 190 (2020), 122248.
[21] A. Phadke, C. Zhang, Y. Hwang, K. Vecchio, S. Varghese, Templated mineralization of synthetic hydrogels for bone-like composite materials: Role of matrix hydrophobicity, Biomacromolecules 11 (8) (2010) 2060–2068.
[22] M. Bongio, M.R. Nejadnik, Z.T. Birgani, P. Habibovic, L.A. Kinard, F.K. Kasper, A. G. Mikos, J.A. Jansen, S.C.G. Leeuwenburgh, J.J.J.P. van den Beucken, In vitro and in vivo enzyme-mediated biomineralization of oligo (poly(ethylene glycol) fumarate hydrogels, Macromol. Biosci. 13 (6) (2013) 777–788.
[23] T.V. Chirila, Zainuddin, Calcification of synthetic polymers functionalized with negatively ionizable groups: A critical review, React. Funct. Polym. 67 (3) (2007) 165–172.
[24] G. Boivin, P.J. Meunier, Effects of bisphosphonates on matrix mineralization, J. Musculoskel Neuron. 2 (6) (2002) 538–543.
[25] M.N. Guven, M.S. Altuncu, T. Bal, D.C. Oran, U. Gulyuz, S. Kizilel, O. Okay, D. Avci, Bisphosphonic acid-functionalized cross-linkers to tailor hydrogel properties for biomedical applications, ACS Omega 3 (8) (2018) 8638–8647.
[26] L. Liu, X. Li, X. Shi, Y. Wang, Injectable alendronate-functionalized GelMA hydrogels for mineralization and osteogenesis, RSC Adv. 8 (40) (2018) 22764–22776.
[27] M. Diba, W.A. Camargo, M. Brindisi, K. Farbod, A. Klymov, S. Schmidt, M. J. Harrington, L. Draghi, A.R. Boccaccini, J.A. Jansen, J.J.J.P. van den Beucken, S. C.G. Leeuwenburgh, Composite colloidal gels made of bisphosphonate-functionalized gelatin and bioactive glass particles for regeneration of osteoporotic bone defects, Adv. Funct. Mater. 27 (45) (2017) 1703438, https://doi.org/10.1002/adfm.v27.4510.1002/adfm.201703438.
[28] S. Kootala, Y. Zhang, S. Ghalib, V. Tolmachev, J. Hilborn, D. Ossipov, Control of growth factor binding and release in bisphosphonate functionalized hydrogels guides rapid differentiation of precursor cells in vitro, Biomater. Sci. 4 (2016) 250–254.
[29] R. Vasita, K. Shanmugam, D.S. Katti, Improved biomaterials for tissue engineering applications: Surface modification of polymers, Curr. Top. Med. Chem. 8 (4) (2008) 341–353.
[30] J. Yang, Y. Mei, A.L. Hook, M. Taylor, A.J. Urquhart, S.R. Bogatyrev, R. Langer, D. G. Anderson, M.C. Davies, M.R. Alexander, Polymer surface functionalities that control human embryoid body cell adhesion revealed by high throughput surface characterization of combinatorial material microarrays, Biomaterials 31 (34) (2010) 8827–8838.
[31] J.H. Lee, H.W. Jung, I.-K. Kang, H.B. Lee, Cell behaviour on polymer surfaces with different functional groups, Biomaterials 15 (9) (1994) 705–711.
[32] J.M. Curran, R. Chen, J.A. Hunt, The guidance of human mesenchymal stem cell differentiation in vitro by controlled modifications to the cell substrate, Biomaterials 27 (27) (2006) 4783–4793.
[33] D.S.W. Benoit, M.P. Schwartz, A.R. Durney, K.S. Anseth, Small functional groups for controlled differentiation of hydrogel-encapsulated human mesenchymal stem cells, Nat. Mater. 7 (2008) 816–823.
[34] M. Lanniel, E. Huq, S. Allen, L. Buttery, P.M. Williams, M.R. Alexander, Substrate induced differentiation of human mesenchymal stem cells on hydrogels with modified surface chemistry and controlled modulus, Soft Matter 7 (14) (2011) 6501, https://doi.org/10.1039/c1sm05167a.
[35] J.E. Phillips, T.A. Petrie, F.P. Creighton, A.J. García, Human mesenchymal stem cell differentiation on self-assembled monolayers presenting different surface chemistries, Acta Biomater. 6 (1) (2010) 12–20.
[36] M.R. Nejadnik, X. Yang, M. Bongio, H.S. Alghamdi, J.J.J.P. van den Beucken, M.C. Huysmans, J.A. Jansen, J. Hilborn, D. Ossipov, S.C.G. Leeuwenburgh, Self-healing hybrid nanocomposites consisting of bisphosphonated hyaluronan and calcium phosphate nanoparticles, 35 (25) (2014) 6918–6929.
[37] M.T. Frassica, S.K. Jones, J. Suriboot, A.S. Arabiyat, E.M. Ramirez, R.A. Culibrk, M. S. Hahn, M.A. Grunlan, Enhanced osteogenic potential of phosphonated-siloxane hydrogel scaffolds, Biomacromolecules 21 (12) (2020) 5189–5199.
[38] S. Altuncu, F. Demir Duman, U. Gulyuz, H. Yagci Acar, O. Okay, D. Avci, Structure-property relationships of novel phosphonate-functionalized networks and gels of poly(β-amino esters), Eur. Polym. J. 113 (2019) 155–164.
[39] P. Ferruti, Poly(amidoamine)s: Past, Present, and Perspectives, J. Polym. Sci. Polym. Chem. Ed. 51 (11) (2013) 2319–2353.
[40] P. Ferruti, S. Bianchi, E. Ranucci, F. Chiellini, A.M. Piras, Novel Agmatine-Containing Poly(amidoamine) hydrogels as scaffolds for tissue engineering, Biomacromolecules 6 (4) (2005) 2229–2235.
[41] E. Jacchetti, E. Emilitri, S. Rodighiero, M. Indrieri, A. Gianfelice, C. Lenardi, A. Podesta, E. Ranucci, P. Ferruti, P. Milani, Biomimetic poly(amidoamine) hydrogels as synthetic materials for cell culture, J. Nanobiotechnol. 6 (14) (2008) 1–15.
[42] E. Emilitri, F. Guizzardi, C. Lenardi, M. Suardi, E. Ranucci, P. Ferruti, Novel poly (amidoamine)-based hydrogels as scaffolds for tissue engineering, Macromol. Symp. 266 (1) (2008) 41–47.
[43] F. Martello, A. Tocchio, M. Tamplenizza, I. Gerges, V. Pistis, R. Recenti, M. Bortolin, M. Del Fabbro, S. Argentiere, P. Milani, C. Lenardi, Poly(amido-amine)-based hydrogels with tailored mechanical properties and degradation rates for tissue engineering, Acta Biomater. 10 (3) (2014) 1206–1215.
[44] J.-P. Montheard, M. Chatzopoulos, D. Chappard, 2-Hydroxyethyl methacrylate (HEMA): chemical properties and applications in biomedical fields, J.M.S.-Rev. Macromol. Chem. Phys. C 32 (1) (1992) 1–34.
[45] Y.S. Casadio, D.H. Brown, T.V. Chirila, H.-B. Kraatz, M.V. Baker, Biodegradation of poly(2-hydroxyethyl methacrylate) (PHEMA) and poly{(2-hydroxyethyl methacrylate)-co-[poly(ethylene glycol) methyl ether methacrylate]} hydrogels containing peptide-based cross-linking agents, Biomacromolecules 11 (11) (2010) 2949–2959.
[46] C.R. Degenhardt, D.C. Burdsall, Synthesis of ethenylidenebis(phosphonic acid) and its tetraalkyl esters, J. Org. Chem. 51 (18) (1986) 3488–3490.
[47] Y.-F. Chou, W.-A. Chiou, Y. Xu, J.C.Y. Dunn, B.M. Wu, The effect of pH on the structural evolution of accelerated biomimetic apatite, Biomaterials 25 (22) (2004) 5323–5331.
[48] M. Liu, J. Chen, Y.-P. Cheng, Y.-N. Xue, R.-X. Zhuo, S.-W. Huang, Novel poly (amidoamine)s with pendant primary amines as highly efficient gene delivery vectors, Macromol. Biosci. 10 (4) (2010) 384–392.
[49] C. Lin, C. Blaauboer, M.M. Timoneda, M.C. Lok, M. van Steenbergen, W. E. Hennink, Z. Zhong, J. Feijen, J.F.J. Engbersen, Bioreducible poly(amido amine)s with oligoamine side chains: Synthesis, characterization, and structural effects on gene delivery, J. Control. Release 126 (2) (2008) 166–174.
[50] T. Bailly, R. Burgada, T. Prangé, M. Lecouvey, Synthesis of tetradentate mixed bisphosphonates-new hydroxypyridinonate ligands for metal chelation therapy, Tetrahedron Lett. 44 (1) (2003) 189–192.
[51] J. Chen, S.-W. Huang, M. Liu, R.-X. Zhuo, Synthesis and degradation of poly(beta-aminoester) with pendant primary amine, Polymer 48 (3) (2007) 675–681.
[52] M. Mastrogiacomo, S. Scaglione, R. Martinetti, L. Dolcini, F. Beltrame, R. Cancedda, R. Quarto, Role of scaffold internal structure on in vivo bone formation in macroporous calcium phosphate bioceramics, Biomaterials 27 (17) (2006) 3230–3237.
[53] Q.Z. Wang, X.G. Chen, N. Liu, S.X. Wang, C.S. Liu, X.H. Meng, C.G. Liu, Protonation constants of chitosan with different molecular weight and degree of deacetylation, Carbohydr. Polym. 65 (2) (2006) 194–201.
[54] K. Kepa, R. Coleman, L. Grøndahl, In vitro mineralization of functional polymers, Biosurf. Biotribol. 1 (3) (2015) 214–227.
[55] I. Rehman, W. Bonfield, Characterization of hydroxyapatite and carbonated apatite by photo acoustic FTIR spectroscopy, J. Mater. Sci. Mater. Med. 8 (1997) 1–4.
[56] A. Shkilnyy, A. Friedrich, B. Tiersch, S. Schöne, M. Fechner, J. Koetz, C.-W. Schläpfer, A. Taubert, Poly(ethylene imine)-controlled calcium phosphate mineralization, Langmuir 24 (5) (2008) 2102–2109.
[57] I. Mayer, R. Schlam, J.D.B. Featherstone, Magnesium-containing carbonate apatites, J. Inorg. Biochem. 66 (1) (1997) 1–6.
[58] Y. Li, X. Chen, A. Fok, J.C. Rodriguez-Cabello, C. Aparicio, Biomimetic mineralization of recombinamer-based hydrogels toward controlled morphologies and high mineral density, ACS Appl. Mater. Interfaces 7 (46) (2015) 25784–25792.
[59] V. Rusu, C. Ng, M. Wilke, B. Tiersch, P. Fratzl, M. Peter, Size-controlled hydroxyapatite nanoparticles as self-organized organic–inorganic composite materials, Biomaterials 26 (26) (2005) 5414–5426.
[60] R.F. Wallin, A Practical Guide to ISO 10993–5, Cytotoxicity (1998).
[61] M.N. George, X. Liu, A.L. Miller, H. Xu, L. Lu, Phosphate functionalization and enzymatic calcium mineralization synergistically enhance oligo[poly(ethylene

glycol) fumarate] hydrogel osteoconductivity for bone tissue engineering, J. Biomed. Mater. Res. A. 108 (3) (2020) 515–527.
[62] G. Hulsart-Billström, P.K. Yuen, R. Marsell, J. Hilborn, S. Larsson, D. Ossipov, Bisphosphonate-linked hyaluronic acid hydrogel sequesters and enzymatically releases active bone morphogenetic protein-2 for induction of osteogenic differentiation, Biomacromolecules 14 (9) (2013) 3055–3063.
[63] J. Tan, R.A. Gemeinhart, M. Ma, W. Mark Saltzman, Improved cell adhesion and proliferation on synthetic phosphonic acid-containing hydrogels, Biomaterials 26 (17) (2005) 3663–3671.
[64] X. Zhang, Y. He, P. Huang, G. Jiang, M. Zhang, F. Yu, W. Zhang, G. Fu, Y. Wang, W. Li, H. Zeng, A novel mineralized high strength hydrogel for enhancing cell adhesion and promoting skull bone regeneration in situ, Compos. Part B: Eng. (2020) 108183.
[65] C. Nuttelman, M. Tripodi, K. Anseth, Synthetic hydrogel niches that promote hMSC viability, Matrix Biol. 24 (2005) 208–218.